Welding Mechanics for Advanced Component Safety Assessment

Dieter Siegele

Fraunhofer Institute for Mechanics of Materials IWM, Wöhlerstr. 11, 79108 Freiburg, Germany

1. Introduction

Welding mechanics is an engineering subject concerned with the mechanics and the material behaviour at welding and in welds. In research and applications the different welding processes, the microstructures resulting in the weld and their properties in terms of deformability, strength, and toughness and the structural behaviour of welded components are considered, especially if welding induced residual stresses and defects are present. The interaction of the parameter fields “process”, “properties” and “defect” for an advanced fitness-for-service assessment of welded components is shown by the triangle in Fig.1.

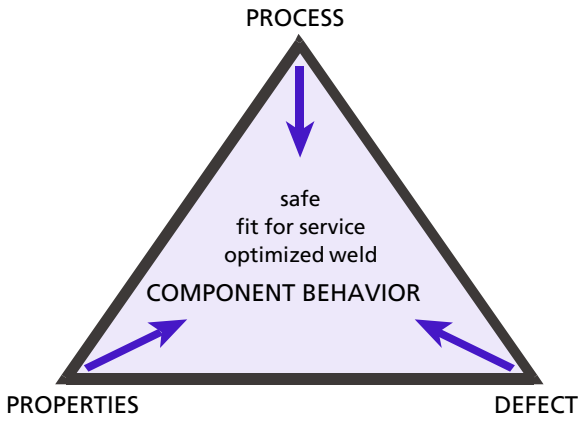

Fig.1: The welding mechanics triangle

The concept of welding mechanics comprises mechanics and material behaviour at welding and in welds; they concern the welding process, the properties resulting in the weld in terms of deformability, strength and toughness and the structural behaviour of welded components, especially if residual stresses and defects are present. In this publication, results of experimental and numerical work in the field of welding mechanics are described. Through examples from automotive, space, nuclear and pipe-line applications it is demonstrated that an equilibrated treatment and a close interaction of "process", "properties" and "defect" are necessary to come up with an advanced fitness-for-service assessment of welded components.

2. Process simulation to control distortions in welded Al automotive components

Distortions and residual stresses induced by welding can impair precise fabrication and assembly and can have a negative influence on strength and lifetime of components and structures. For a thin walled light weight automotive structure such effects have been investigated and quantified using advanced material modelling and FE simulation [1].

The automotive component investigated is a section of the space frame structure of an AUDI car (Fig.2) consisting of an extruded and hydro-formed AlMgSi0.5 (ENAW6060, T7) roof profile and a modified AlSi10Mg (ENAC4300) = AURAL-2 ® die-cast B-pillar connected by three partial Laser (LB)-welds. Consumables S-AlSi12 are used in the series production; no post weld heat treatment is applied.

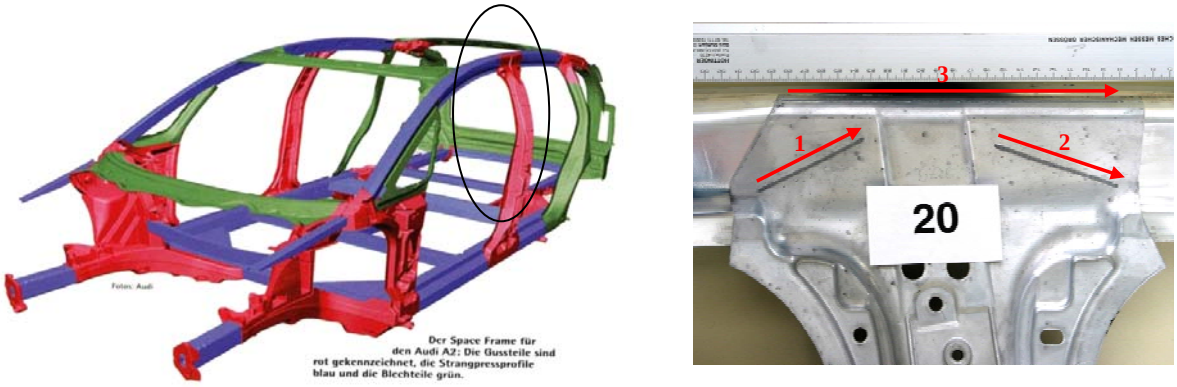

Fig.2: Space frame structure of AUDI A2 and detail of connection between B-pillar and roof profile

For the numerical simulation of process and structure the commercial finite element code SYSWELD® has been used which consists of a thermo-metallurgical and a mechanical analysis package. The necessary input data – physical and mechanical material properties as a function of temperature – have been determined experimentally using miniature specimens extracted by spark erosion technique from base metals (BM), weld metals (WM) and heat affected zones (HAZ) of representative weld joints. As an example, Fig.3 shows measured yield stresses and true stress-strain curves for the LB-welded extrusion profile.

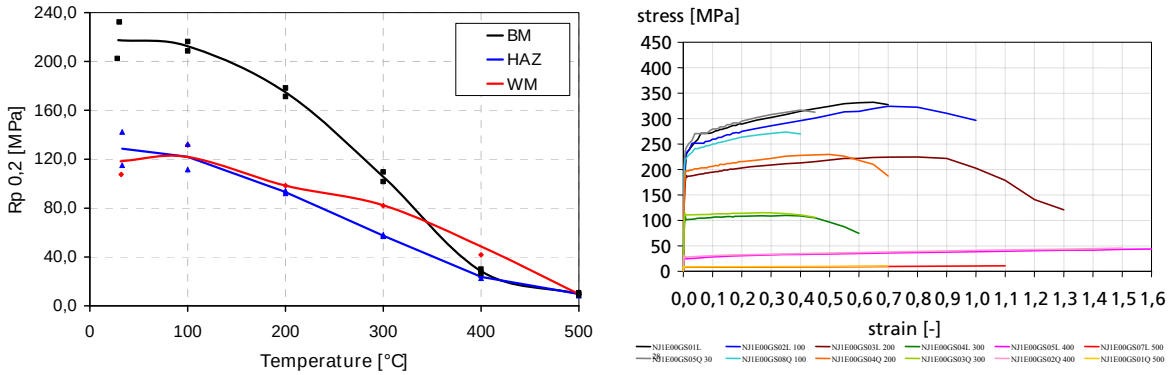

Fig.3: Yield stress $R_{p0.2}$ vs. temperature for different material zones in ENAW6060, T7 – laser weld, and true stress-strain curves at temperatures from RT to 500°C

An equivalent heat source moving in the welding direction has been used to model the complex heat transfer, melting and fluid dynamics processes in the torch and the melt pool, the geometry and intensity of which has been calibrated by comparing calculated temperature distributions with thermocouple measurements during welding and with melt zone geometries derived from metallographic sections of real welds. Very good agreement between measured and calculated temperature profiles concerning peak temperature and cooling rate are received if for the standard heat source model with Gaussian distribution of energy density over the depth a lower heat conductivity in the transverse as compared to the longitudinal direction in the weld pool is assumed. Fig.4 shows temperature vs. time curves measured with thermocouples at different distances from the weld centre line in comparison with FE results after fitting the anisotropic heat source model. The close correspondence between the macro sections of the real weld and the calculated contour of the melting isotherm in Fig.5 also shows the good quality of the simulation.

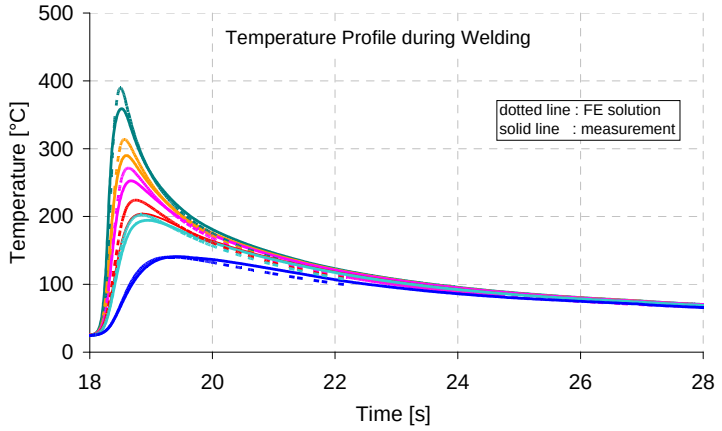

Fig.4: Calculated and measured temperature profiles for LB-weld No.1 in automotive structure

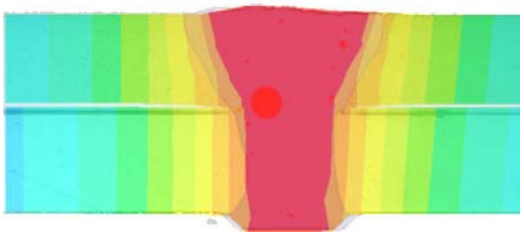

Fig.5: Calculated and measured melt pool geometries; red: calculated – temperatures above melting at 600°C, grey: derived from macro-sections

The structural model of B-pillar, roof profile and 3 single V LB-welds consists of about 155000 8-noded solid elements (4 over the width of the weld); shell elements are used in addition to model heat transfer by convection and radiation; the constraint conditions during welding have been modelled by spring elements at nodes corresponding to the positions of the clamping devices in production; after completion of the welding process and cooling down the boundary conditions at the supported nodes have been released and resulting distortions and residual stresses have been evaluated. On a 64 Bit computer (HP Alpha ServerES40 with 10GB working storage) about 110 hours of computing time were required for the simulation of the three LB-welds.

Thermal and mechanical calculations are done in an uncoupled manner. Fig.6 as an example shows the temperature fields in the structure at a certain time instant during LB-weld No.1, 2 and 3.

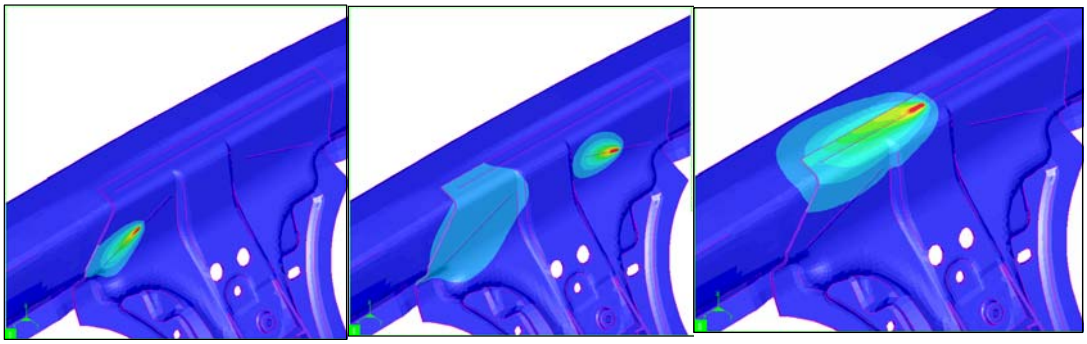

Fig.6: Calculated temperature fields at different selected times in LB-welds No.1-3

For the mechanical simulation a simplified Grong model and elastic, ideally-plastic material behaviour have been used attributing strength properties as measured to the local material zones acc. to their temperatures. In Fig.7 calculated displacements after release of the clamping devices are plotted in comparison with the original geometry. Large displacements due to

shrinkage forces especially at both ends of the roof profile occur; the magnitude of 4 mm found corresponds quite well with measurements on a structural part taken from series production.

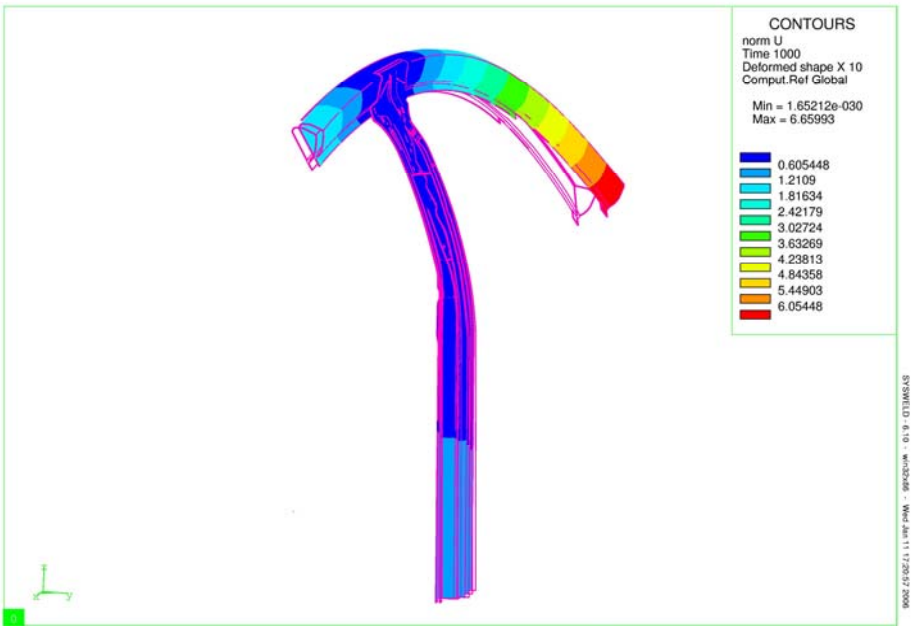

Fig.7: Calculated distortion after welding sequence 1-2-3 and release of clamping devices in comparison with original component geometry (line contours)

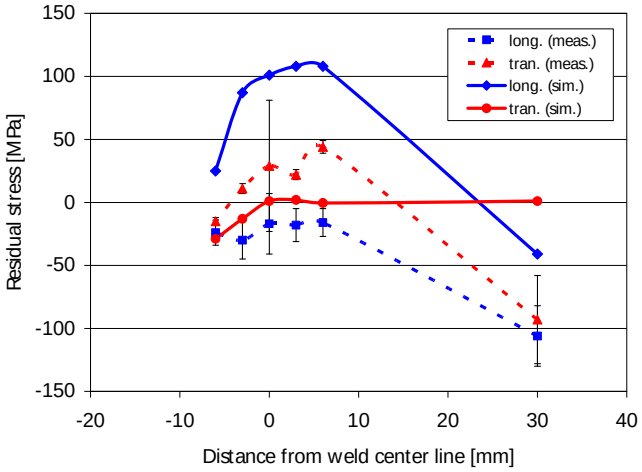

Fig.8: Transverse and longitudinal residual stresses on the side of the cast B-pillar in LB-weld No.3 – comparison between calculated (solid lines) and measured values (dashed lines)

In Fig.8 calculated longitudinal and transverse residual stresses across the LB-weld No.3 are compared with X-ray measurements on a series production component. Whereas the calculated transverse stresses are very small, the longitudinal stresses show high tensile stresses in the weld and small compression stresses in the base metal. On the other hand, the measurements show

comparable stress profiles with small differences in the transverse stresses and larger ones in the longitudinal stresses; especially, compression stresses are found in the weld and the (cast) base metal. The differences may result from an unknown initial stress state in the extruded and the cast parts and from additional forces of the laser beam head on the weld which have not been considered in the simulation.

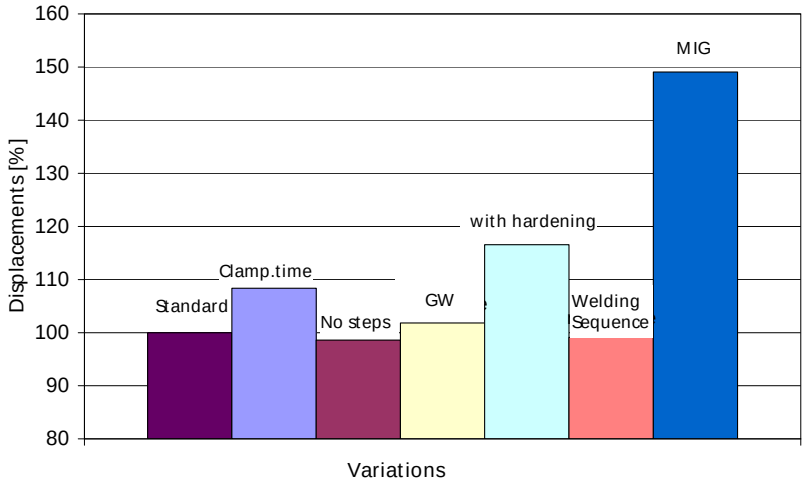

Fig. 9: Maximum calculated displacement at the end of the roof beam for the investigated parameter variations [2]

Using an improved heat source model (adjusted to measured temperature profiles and macro-sections assuming anisotropic thermal conductivity in the melt pool) a series of simulations has been conducted to study the influences of different parameters on the accuracy of the calculated distortions. Fig. 9 shows typical results. Compared to the LB-weld, here taken as reference, the biggest influence of about 50% comes from an increased heat input as in the example of an analysed MIG-weld. The heat input corresponds to the load in structural mechanics and a reliable simulation result can only be expected if the heat input is sufficiently well known. Next the material properties are important: There is a 16% influence if isotropic material hardening is taken into account instead of using the elastic, ideally-plastic material description. If uniform instead of zone-specific material properties for WM and HAZ are used an influence of 12% results (for the Aluminium LB-weld!). If parameters of the welding process are varied a distinct influence is found from shortening the time interval between finishing the weld and opening the clamping devices: distortions are increased for shorter hold times because at higher temperatures there is less time for plastic relaxation in the weld. In addition, a minor increase of 10% for the predicted distortion results if the welding sequence is changed for example from 1-2-3 to 3-2-1.

The choice of the time step in the calculation of temperatures, distortions and residual stresses was found of minor importance; acceptable results are found by choosing time steps smaller than 0.5 of weld pool length over welding speed.

In summary, the investigations demonstrate that using adequate material properties and validated heat source modelling the numerical simulation is able to describe the development of welding residual stresses and distortions also in complex components. It allows for the systematic study of the influence of welding process parameters and the results can be directly used to optimize production.

3. Material properties characterisation to verify damage tolerance concept for EB-weld

In the course of the process to replace shear bolt connections in the ARIANE 5 booster cases by EB-welds a detailed analysis of the safety and reliability implications has been required. The optimized EB-weld is performed without consumables in the shell (diameter 3 m, wall thickness 12 mm) made of the martensitic steel CrMoNiV4 10 steel (D6AC); cosmetic passes are used on both surfaces; the welding is done in the final Q&T state of the shell with only local post weld heat treatment. For the application of a damage tolerance concept representative stress-strain and fracture toughness data had to be determined [3].

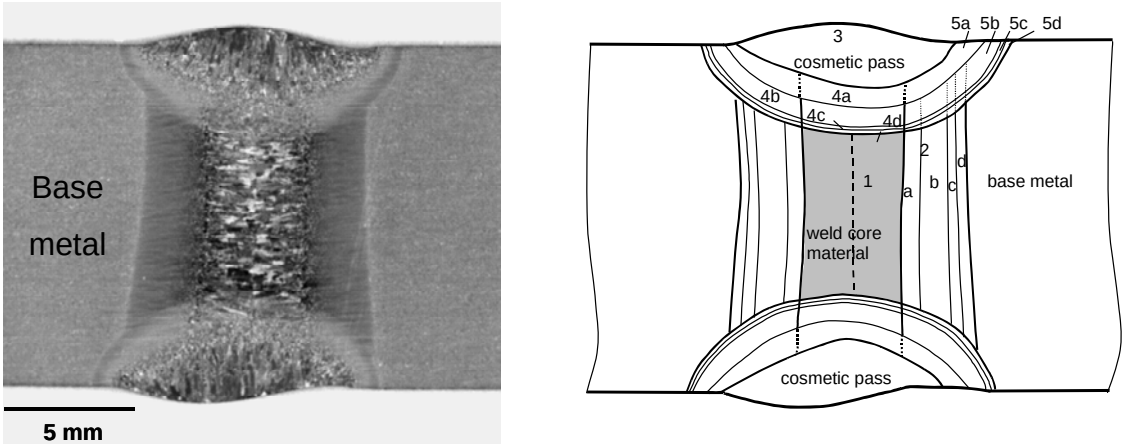

Fig.10: Macrograph of EB-weld cross section for ARIANE 5 booster with main zones of interest

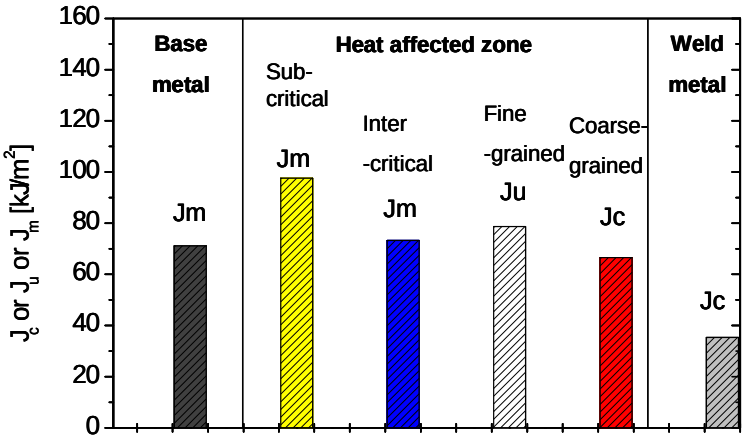

Fig.11: Fracture toughness at RT of different micro-structural zones in ARIANE 5 booster EB-weld

Single edge notched three point bend specimens (10x10mm) with through the thickness initial cracks of a_0/W were extracted by spark erosion technique from a real weld and have been tested at room temperature acc. to BS 7448. Under metallographic control the crack tips had been carefully positioned in different zones of the weld. Fig.10 shows details of the complex microstructure. To characterize some very small zones like coarse grained (marked (2a) in Fig.10, fine grained (2b), inter-critically reheated (2c) and sub-critically reheated (2d)) HAZ representative substitute material has been produced with a Gleeble weld simulator which then has allowed full size testing.

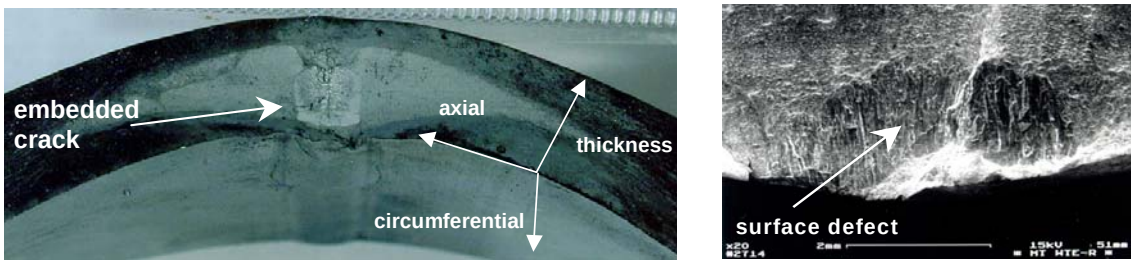

Fig.12: Defects in EB-welded D6AC model-vessels before burst testing

Results of the fracture testing in terms of critical J-values are shown in Fig.11. Significant differences are revealed which normally cannot be identified by integral tests; they range from brittle fracture instability (J_c) in weld metal and coarse grained zone to ductile stable crack growth without (J_m) or with instability (J_u) in other parts of the weld. Sub-scale model vessel (inner diameter 425mm, wall thickness 12mm) burst tests have been performed and numerically

evaluated to validate the material description and the applied failure prediction concepts. Fig.12 shows a natural embedded and a surface defect in two of the investigated model vessels.

High resolution FEM analyses have been evaluated for tensile stress distribution and stress tri-axiality at the crack front as well as the energy-integral J as a function of geometry (vessel, defect) and loading (internal pressure). Predictions of failure have been made using ductile and brittle fracture concepts. The Gurson model for ductile damage and the two parameter approach J_c vs. constraint C have been used together with local material toughness from fracture toughness tests on surface-cracked tensile specimens and $C = \sigma_{mean}/\sigma_{equivalent}$ from the FE calculations. To apply the Ritchie/Knott/Rice model for cleavage damage critical crack tip distances and brittle fracture stresses have been determined in separate notched round bar tension tests. Fig.13 shows one of the model vessels after burst testing and a comparison of experimental and numerical results. The agreement with a 10% conservatism is very good – especially when taking into account that the natural defects have been modelled as sharp cracks and that the lower bound weld core instead of the real local toughness has been used.

Vessel / Defect	***Burst Pressure***	***Numerical Prediction***	
		J-Concept	***RKR Model***
Vessel 1 Embedded Defect	93 MPa	81 MPa	78 MPa
Vessel 2 Surface Defect	100 MPa	90 MPa	95 MPa

Fig.13: Sub-scale pressure vessel No.2 with surface defect after burst test and comparison of experimental and calculated burst pressures

In summary, the investigations have shown that based on the verified combined brittle/ductile failure prediction concept a local fracture toughness evaluation could be used to screen the fracture toughness properties of the individual welds and define worst case positions of possible

defects. These worst case defects were assessed by FEM-analyses and safety margins could be quantified for undetected hypothetical defects; this helped to reduce NDE-efforts.

4. Fitness-for-service assessment of a BWR core shroud weld with cracks and residual stresses

In the welds of core shrouds of nuclear boiling water reactors (BWR) the initiation and extension of crack like defects can not be completely excluded because of possible corrosion and irradiation processes. To proof the integrity of the structure over the life time non destructive examination and a fracture mechanics based assessment are required in such cases. For detected or postulated cracks the welding residual stresses represent the dominant loading. Therefore the knowledge about distribution and magnitude of the residual stresses from measurement or calculation is of utmost importance for the residual life of the shroud. In the study reported here the welding process has been simulated to calculate residual stresses in the component and to use such loading as input to a fracture mechanics analysis [4].
Fig.14 shows the finite element model of the relevant section of the core shroud geometry with the two thin shells surrounding the reactor core made of steel 1.4550 (X10CrNiNb18 9) connected to a flange ring by two circumferential welds.

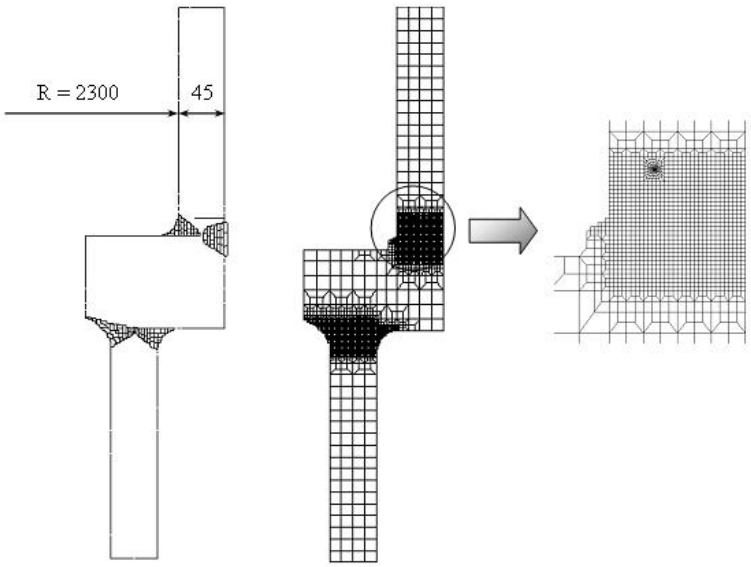

Fig.14: Geometry of the core shroud with weld passes and finite element mesh

The finite element code ABAQUS has been used for the numerical simulation of the welding process; axis symmetry has been assumed. Following the welding protocol a total number of 95 MMA- or SAW-passes have been inserted in the structural model one after the other in the upper and lower weld; a melting temperature of 1600°C and process specific hold times for all elements of one pass have been taken into account. To evaluate the residual stresses after a stress relief treatment and grinding the weld root region conservatively a non linear kinematic hardening material law has been used with parameters derived from tensile tests at temperatures from RT to 1000°C. Fig.15 shows results for the calculated axial residual stresses. In the relevant cross section without crack there is an equilibrium distribution with maximum tensile stresses of 250MPa at the cylinder surfaces and compression stresses in the middle part of the wall.

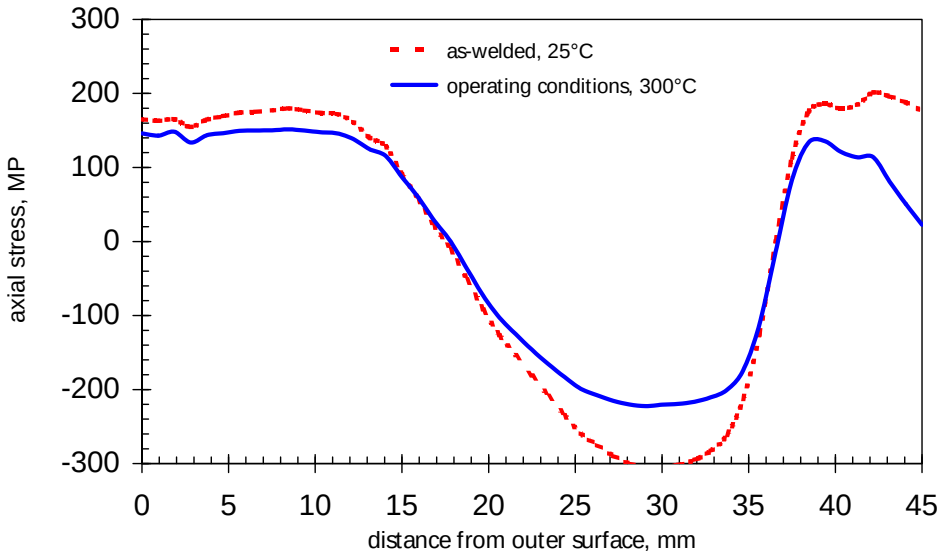

Fig.15: Residual axial stresses in the flange weld at room and at service temperature

A full circumferential crack extending from the outer surface into the HAZ of the upper weld with a constant depth has been assumed for the fracture analysis in the residual stress field. Stress intensity factors (SIF) have been calculated for different crack depths using a weight function approach [5]. The analytical solutions have been verified also by a complete numerical (node release technique and extrapolation of CMOD) evaluation. Fig.16 shows very good agreement between analytical and numerical results; the SIF is positive and the crack stays open for all investigated depths (see picture to the right) – even in the part of the cross section that showed compression stresses without the cut (compare Fig.15). The SIF distribution tends to zero at break through. Fig. 16 also demonstrates the influence of different material models on the distribution of SIF. The more realistic nonlinear hardening model tends to higher SIF than the linear hardening model.

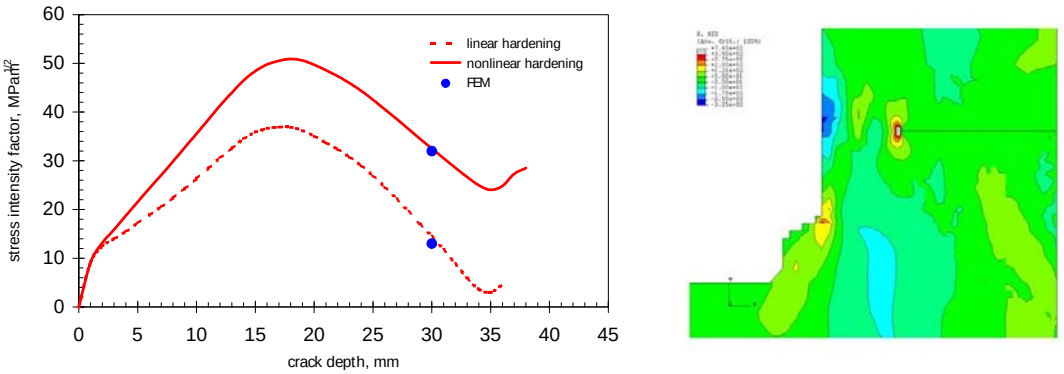

Fig.16: Stress intensity factors for circumferential, constant depth cracks located at the outer surface in the HAZ of the upper core weld – right: redistribution of axial residual stresses due to 41.3mm deep crack

In summary: Based on the results of weld simulation, residual stress evaluation and fracture mechanics analyses the possible extension of inter-granular stress corrosion cracks in the core shroud welds has been predicted by integrating laboratory measured material crack growth curves da/dt as a function of SIF. Using these results a NDE-strategy has been defined which fulfils the safety requirements of the Technical Rules and the surveillance agency.

4. Defect assessment in pipelines using the German FKM-Guideline "Fracture Mechanics Proof of Strength"

In parallel with efforts in other countries the "FKM Guideline "Fracture Mechanics Proof of Strength" has been developed in Germany in recent years [6, 7]. This "FKM Guideline: Fracture Mechanics Proof of Strength for Engineering Components" is a result of a joint activity between academia, research institutes and industry under the organisation of the Research Committee on Mechanical Engineering (FKM) and has been financially supported by the German Federation of Industrial Research Associations "Otto von Guericke" (AIF).The Guideline is part of a system of proofs of strength which includes the conventional static and the fatigue strength proof for ferrous materials and Al-alloys as well as that for corrosion. This document was first published in 2001; the latest 3rd edition of 2009 includes new topics – e.g. mixed mode and dynamic (impact) loading and others- and it gives additional examples of application [8]; the procedures and solutions have been implemented in the computer program Fracsafe [9]. The Guideline is now widely used in German industries.

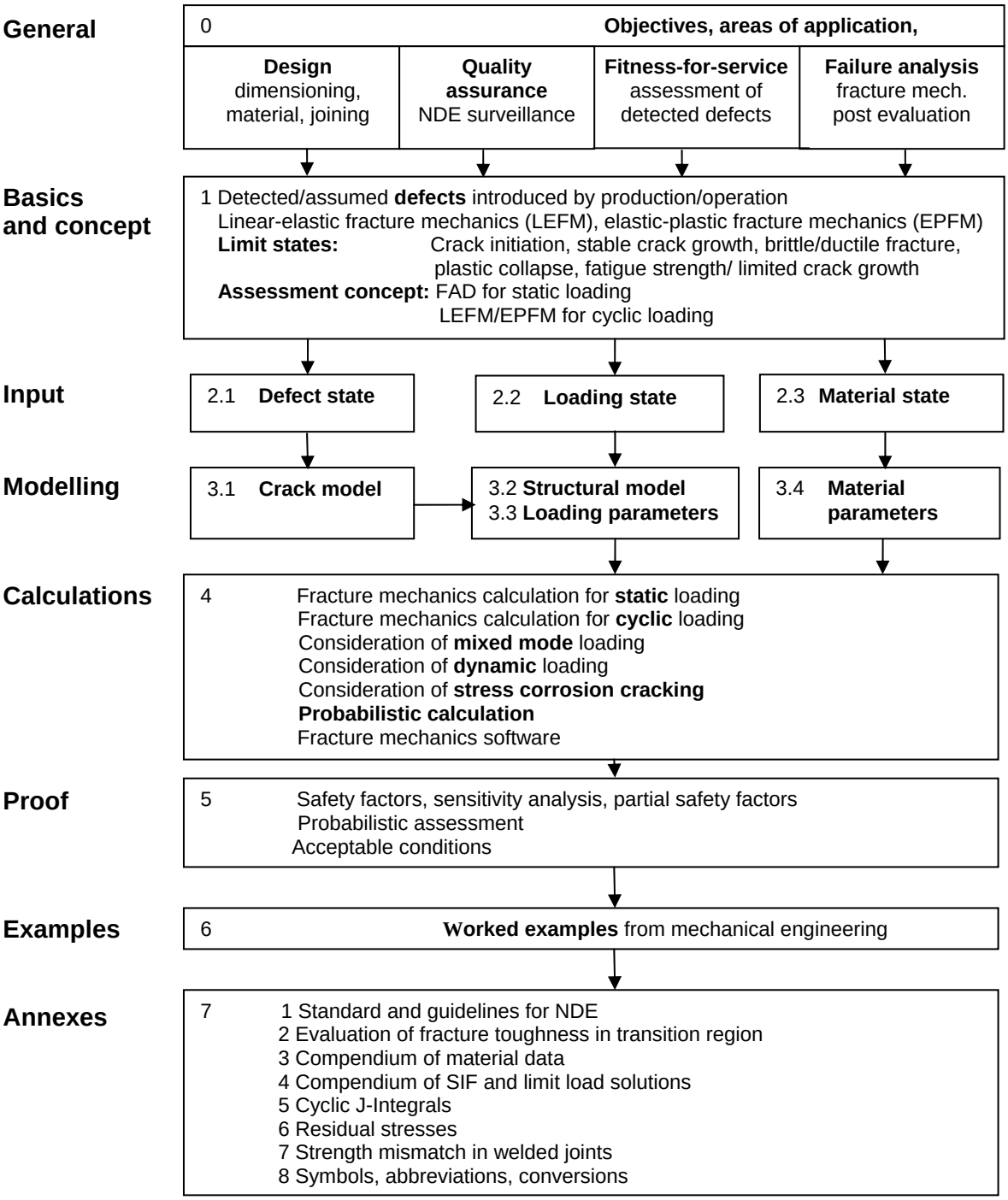

Fig.17: Structure of the FKM Guideline "Fracture Mechanics Proof of Strength for Engineering Components", 3rd edition 2005 [8]

The structure of the document is shown in Fig.17. As listed in **General** (Guideline Chap.0)**,** different tasks can be handled by the concept of the Guideline following the same sequence of working steps. The **Basic Concept** (Chap.1)for the proof of strength - as e.g. in API 579(2000), SINTAP (1999) or WES 2805(1997) - is the failure assessment diagram(FAD) using the elastic-plastic parameters K_r and L_r and material parameters K_{mat} for limiting cases crack initiation, stable growth and instability. For fatigue loading LEFM is applied with ΔK the cyclic stress intensity factor and the crack growth rate da/dN as well as the threshold value ΔK_{th} as material parameters. The main steps of the solution are:
Collecting and describing **Input** quantities (Chap.2)
- defect state by non-destructive examination (fabrication-, service-, and hypothetical defects)
- loading state (external forces and moments, internal pressure, thermal and residual stresses) and
- material state (material properties in the component under its specific service conditions).

Modelling (Chap.3) of these component states by planar cracks with geometrically simple boundaries in reference planes normal to the principal stresses in substitute structures which allow calculation of the FAD parameters K_r and L_r from available collections of formulae in appendix 7.4 of this Guideline; the fracture toughness K_{mat} and the geometry independent but material specific failure line have to be derived from fracture mechanics experiments or correlations; all steps of this modelling procedure have to be conservative.
Calculating (Chap.4) the component state for the specific geometrical (structure and defect) and loading conditions; new aspects (since 1st edition) are marked and
assessing the component state (**Proof** Chap.5) by a comparison to »basic« or »advanced« failure lines depending on the yielding characteristics of the material (also in welds); reserve factors can be evaluated to quantify the safety margin against brittle or plastic failure; a probabilistic treatment is possible.
A collection of 20 **Worked examples** covering typical engineering components as shafts, plates, pipelines, casings and tracks as well as 8 **Annexes** support the user in executing the different steps of the Guideline for design, quality assurance, fitness for service and failure analysis.

The assessment of defects in a spiral welded pipe line is one of the examples for the application of the Guideline. Indications of defects were found during inspection of the pipeline; they have been induced by local cold forming of excess weld metal during treatment of the welded pipe for external isolation; the defective zones extended over several cm in length and had a depth of up to 2mm from the outer surface; in a worst case consideration these zones have been treated

as being cracks. Fig.18 shows the geometry and loading conditions for the applied structural model. Following the Guideline procedure a critical crack depth at service internal pressure 7.6 MPa a_c = of 3.4mm in the 16mm wall has been calculated; and this resulted from a FAD instability analysis using a minimum fracture toughness of K_{mat} = 20 MPa√m derived from CTOD tests on real HAZ specimens. Performing a fatigue analysis conservatively assuming an infinitely long initial crack with a depth of a_0 = 2mm has shown that the critical crack depth could only be reached in a multiple of the lifetime with exaggerated internal pressures amplitudes in the pipe line. The calculated reserve factors in load, crack size and toughness shown in Fig. 19 have been rated sufficient and the 2mm defects to be acceptable.

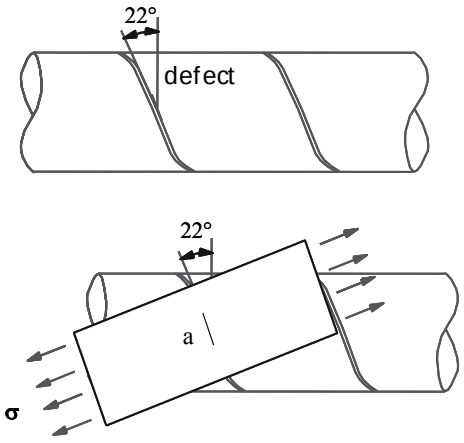

Structural model: plate with surface crack

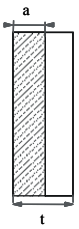

at service internal pressure p = 7.6 MPa

t [mm]	σ_{ax} [MPa]	σ_t [MPa]	τ [MPa]	σ [MPa]
15.6	342.1	167.3	60.8	191.8
18.6	286.3	139.4	51.1	143.8

Fig.18: Assessment of a defect in spiral welded pipe (FKM Guideline [8], worked example No.7)

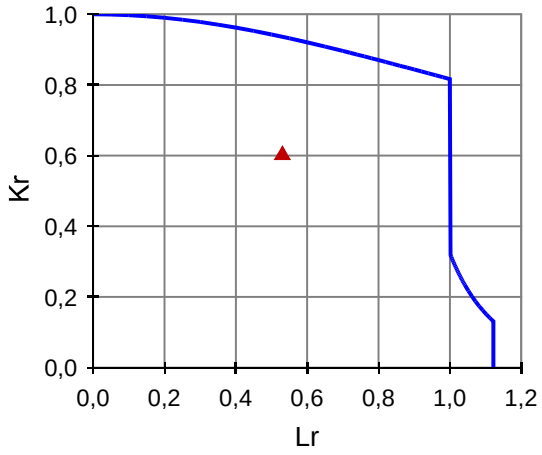

- Reserve factor in load

  f_F = 14.3 MPa / 7.6 MPa = 1.88

- Reserve factor in crack depth

  f_a = 3.4 mm / 2 mm = 1.7

- Fatigue crack extension negligible

Fig.19: Fracture mechanics proof of strength for spiral welded pipe with crack like defect

The limit state function has been chosen here acc. to SINTAP for a material with discontinuous yielding. Such deterministic results have been supplemented by a probabilistic study taking into account that the input data defect (probability of detection (POD), depth of crack model) and material state (fracture toughness in zone of defect) show a certain statistical variation. The parameter load (pressure in the pipe) is preferably treated as a deterministic parameter; however, uncertainties in the size of residual stresses as well as random amplitude fatigue loading could be rationally resolved by using statistical methods. Monte Carlo simulations have been executed to calculate failure probabilities assuming different statistical distributions for the crack depth, the primary and secondary stresses, the yield and the ultimate strength, and the fracture toughness. Results are shown in Fig.20. Using MCS with 10^3 to10^6 simulations, failure probabilities of $P_f = 4\times10^{-3}$ and $P_f = 3\times10^{-2}$ were calculated for the mean crack depth μ_a = 2mm and μ_a = 3mm at the lowest toughness.

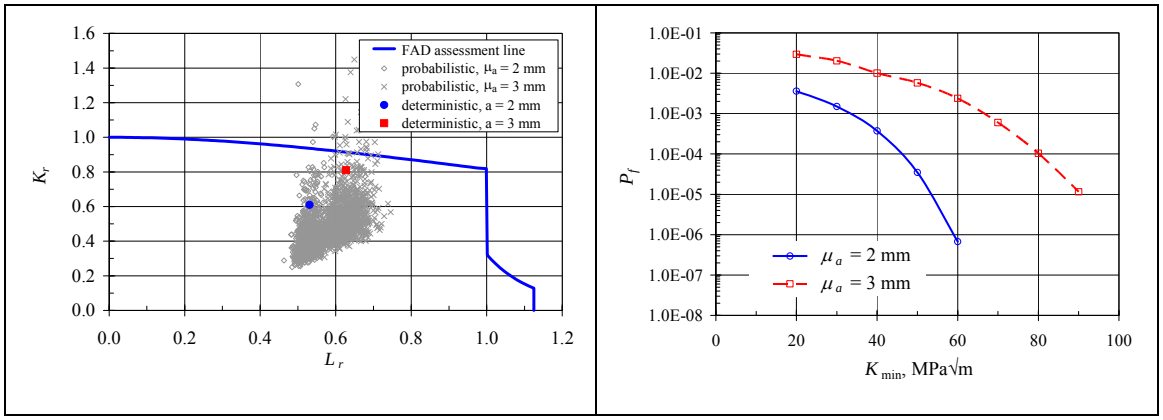

Fig.20: Probabilistic failure assessment of defects in spiral welded pipe line- influence of statistical distribution of defect sizes a and of fracture toughness K_{mat}

In summary: The German FKM-Guideline "Fracture mechanics Proof of Strength for Engineering Components" is based on national and international reference documents and recent research results; the third edition of 2009 [8] includes new topics which allow for the consideration of sequence and overload effects at cyclic loading, mixed mode loading, dynamic (impact) loading, stress corrosion cracking, and probabilistic aspects in fracture mechanics calculations.

6. Summary and conclusions

New results of experimental and numerical work in the field of welding mechanics have been described. The examples are from automotive, space, pipe-line and nuclear applications each

with special emphasis on either "process", "properties" or "defect" and their influence on the behaviour of welded components.

The investigations on the door pillar / roof profile connection have demonstrated that the laser beam welding process can be realistically simulated if adequate material properties and an advanced heat source model are used together with the Code SYSWELD; quantitative results have been derived for the developing welding residual stresses and distortions which are in good agreement with measurements on series components; the numerical model allows for a systematic study of the influence of welding process parameters and the results have been directly used to optimize production.

The investigations on electron beam welds in high strength steel shells have validated a local material properties evaluation which has been used to screen the fracture toughness of individual EB-welds of the ARIANE rocket booster and together with a combined brittle/ductile failure prediction concept to define worst case positions of possible defects. These worst case defects in the component have been assessed by FEM-analyses and safety margins could be quantified for undetected hypothetical defects; this damage tolerance concept also helped to reduce NDE-efforts.

The numerical simulation of praxis relevant multi-pass MMA/SAW-welds has demonstrated that it can deliver residual stresses to be used in the assessment of cracks; based on such results the possible extension of inter-granular stress corrosion cracks in a NPP core shroud weld has been quantitatively analysed by integrating laboratory measured material crack growth curves da/dt as a function of residual stress induced stress intensity factors; using these results a NDE-strategy has been defined which fulfils the safety requirements of the Technical Rules and the surveillance agency.

A new version of the German FKM-Guideline “Fracture mechanics Proof of Strength for Engineering Components” has been introduced and the underlying fracture mechanics procedures have been demonstrated in an assessment of defects in spiral welded pipes – including a probabilistic treatment of input parameter defect size and fracture toughness.

To come up with a reliable fitness-for-service assessment of a component an equilibrated treatment and a close interaction of the parameters “process”, “properties” and “defects” is required.

7. References

1. Siegele, D. Brand, M. and Veneziano, C.: Numerical welding simulation of an aluminium automotive component, IIW Doc. X-1599-2006
2. Veneziano, C. et al: Numerische Simulation von Verzug und Eigenspannungen geschweißter Komponenten aus Al-Guss und –Strangpressprofilen, Project AIF 13.716N/DVS 9.032, Report S6/ 2006 Fraunhofer IWM Freiburg Febr.2006
3. Windisch, M., Clormann, U., Grunmach, R. Burget, W.,and Sun, D.-Z.: Damage tolerance verification concept of the ARIANE 5 booster welding interface, Proc.Europ.Conf.on Spacecraft Structures, Materials and Mechanical Testing, Noordwijk Nl, Nov.29. – Dec.1.2000 (ESA Sp-468, March 2001)
4. Varfolomeyev, I., Siegele, D. and Beukelmann, D.: Analysis of residual stresses and assessment of postulated cracks in a core shroud weld, ASME Pressure Vessels&Piping Conference, PVP, Vancouver, 4-8 August 2002
5. Varfolomeyev, I.: Weight function for external circumferential cracks in hollow cylinders subjected to axissymmetric opening mode loading, Engng. Fracture Mechanics, Vol.60, pp333-339
6. Blauel, J.G., Burget, W.,Hodulak, L.,Siegele, D.: Assessment of defects in pipelines using the German FKM-Guideline »Fracture Mechanics Proof of strength«, WTIA Conf. Sydney2005
7. Berger,C., Wurm, B., Blauel, J.G., Hodulak, L., Gerdes, C.P.: Fracture mechanics proof of strength of engineering components - A general guideline , ICF 10,2000
8. FKM Guideline „Fracture mechanics proof of strength for engineering components“, version 3, 2009, VDMA Publisher house
9. FracSafe, Software for FKM Guideline “Fracture mechanics proof of strength for engineering components”, Version 2.1, 2009